Improving kinematic wave routing scheme in Community Land Model

Aizhong Ye, Qingyun Duan, Chesheng Zhan, Zhaofei Liu and Yuna Mao

ABSTRACT

Version 3.5 of Community Land Model (CLM) has incorporated a river routing module, called the River Transport Model (RTM), to simulate the runoff routing process over a hydrologic basin. RTM treats river routing as a linear reservoir process propagated through a gridded domain. Because the flow velocity at each grid is set as a constant, RTM cannot simulate river routing well. In this paper, we developed a large scale catchment-based kinematic wave routing (KWR) model to be coupled with CLM, which simulates the movement of water through floodplains and river channels. An advantage of KWR over RTM is that the flow velocity is calculated by the Manning equation, which considers the difference in friction slope and hydraulic radius in each sub-basin (or grid) and time step. A second advantage is that the KWR velocity parameterization accounts for spatial–temporal variability. Using the daily runoff simulations in continental China over the time period 1995–2004 from CLM3.5 as inputs to both RTM and KWR, we found that the simulated discharge of KWR is closer to observed discharge than that of RTM. Our study has shown that KWR may be a valid alternative to RTM in CLM.

Key words | catchment-based kinematic wave routing, China, Community Land Model, discharge, River Transport Model

Aizhong Ye (corresponding author)
Qingyun Duan
Yuna Mao
State Key Laboratory of Earth Surface Processes and Resource Ecology,
College of Global Change and Earth System Science,
Beijing Normal University,
Beijing 100875,
China
E-mail: *Azye@bnu.edu.cn*

Chesheng Zhan
Zhaofei Liu
Key Laboratory of Water Cycle and Related Land Surface Processes,
Institute of Geographical Sciences and Natural Resources Research,
Chinese Academy of Sciences,
11A Datun,
Beijing 100101,
China

INTRODUCTION

Land surface processes play an important role in the climate system (Oki *et al.* 2001; Oki & Kanae 2006). The interaction between land surface and atmosphere affects how water and energy fluxes are exchanged across the land surface. The runoff from the land surface determines the freshwater inflow into the ocean, which in turn influences the salinity and hydrothermal exchanges between the ocean, sea ice and the atmosphere. Land surface models (LSMs) are an indispensible tool for understanding how land surface processes interact with the entire climate system. The Community Land Model (CLM) is one of the most commonly used and state-of-the-art LSMs available today. The current version CLM Version 3.5 (CLM3.5) has undergone numerous upgrades from the original Common Land Model developed by Dai *et al.* (2003) in areas such as carbon cycling, vegetation dynamics, and river routing. In particular, a river routing model called River Transport Model (RTM) has been incorporated in CLM3.5 to simulate fresh water inflow into the oceans. RTM routes CLM generated total runoff (i.e., the sum of surface and sub-surface runoff) from each modeling grid to the nearest stream and then from upstream to downstream and ultimately to the ocean (Oleson *et al.* 2008). A well-performing RTM can provide reasonable simulation of floods and droughts over the land and generate accurate estimates of freshwater inflow into the ocean (Dai *et al.* 2003).

Most routing models are usually based on the de Saint Venant equation or their approximations such as kinematic wave, noninertia wave, gravity wave and quasi-steady dynamic wave (Yen & Tsai 2001). Paiva *et al.* (2011) presented a large scale geographic information system (GIS) based hydrologic model that solves the full de Saint Venant equation using an explicit finite difference scheme (Keskin *et al.* 1997; Cunge 1999). Bajracharya & Barry (1997) showed that a linearized diffusion approach, which is derived from the de Saint Venant equation without considering inertia terms, can be used to accurately

doi: 10.2166/nh.2012.145

simulate flood routing in river channels. Using an empirical three-parameter relationship between average reach velocity and discharge based on observation data, Beven (1979) developed a generalized kinematic channel network routing model. Jain & Singh (2005) developed an overland flow routing model using the diffusion wave equation based on digital elevation model (DEM).

Solving the full de Saint Venant equation can be quite expensive, therefore Muskingum-type methods, which are based on simplified de Saint Venant equations, such as Extended Muskingum (Kumar *et al*. 2011) and Muskingum–Cunge (Ponce *et al*. 1996), are the commonly used approach to calculate unsteady flow in open river channels (Kshirsagar *et al*. 1995; Ponce *et al*. 1996; Birkhead & James 1998, 2002; Kumar *et al*. 2011). However some researchers consider Muskingum type methods less suitable for large scale floodplain runoff routing (Gong *et al*. 2009). Using the de Saint Venant equation approach, Biancamaria *et al*. (2009) applied LISFLOOD-FP developed by Bates & De Roo (2000) to the Ob River basin in Siberia. The runoff routing over the basin was done on the total runoff integrating pathways (TRIP), a global river channel network at $1^{\circ} \times 1$ resolution (Oki & Sud 1998). Since there are several possible flow directions in a large grid (see Figure 1), the runoff routing results may contain significant uncertainty.

There are a number of popular routing methods which are not based on the de Saint Venant equation. Runoff routing using a unit hydrograph (UH), a simple approach that treats each modeling element as a linear system (Perumal *et al*. 2007), has been used in catchment hydrology and in land surface modeling to simulate streamflow discharge

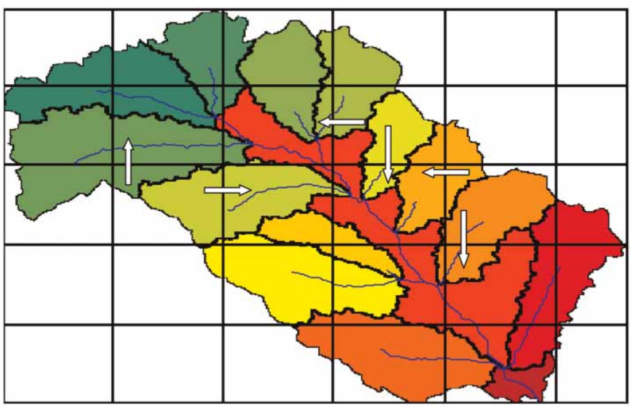

Figure 1 | Flow direction over grids and sub-basins.

(Lohmann *et al*. 2004). Routing methods based on the concept of multi-linear reservoirs are often used in large scale land surface modeling (Camacho & Lees 1999; Zhang *et al*. 2002; Du *et al*. 2003), and the literature has shown that this approach can produce routing simulations comparable to that of the full de Saint Venant equation (Perumal 1994; Camacho & Lees 1999). Du *et al*. (2009, 2010) develop a storm runoff routing approach based on time variant spatially distributed travel time method, in which the calculation of travel time was done using Manning's equation.

When a routing model is run within the context of a climate model, a number of issues need to be considered. First, climate models generally run over a large gridded domain and has a coarse spatial resolution (i.e., >10s of km). Second, climate models are generally run at very fine time steps (say 30 min or less) for accurate representation of the diurnal thermohydrological cycle, while the streamflow data for validating a routing model are often available at only monthly time scale. Even when daily streamflow data are available, they are usually contaminated by anthropogenic factors such as reservoir regulations and/or water diversions and cannot be used directly to validate the routing model (Döll & Lehner 2002; Döll & Siebert 2002; Nilsson *et al*. 2005; Hanasaki *et al*. 2006; Sperna Weiland *et al*. 2010; Wisser *et al*. 2010; Falloon *et al*. 2011). For these reasons the routing models used in land surface modeling are usually simple and many of them are also grid based (Miller *et al*. 1994; Bosilovich *et al*. 1999; Bell *et al*. 2007; Best *et al*. 2011; Falloon *et al*. 2011). Routing is generally accomplished in two steps: grid or slope routing to route runoff from each grid to the nearest river and river routing to route water from upstream to downstream (Gusev & Nasonova 2000). Goteti *et al*. (2008) presented a catchment-based routing model, which operates firstly in floodplains and then in river channels and found that catchment-based routing performs better than grid-based routing.

The main error sources of routing schemes in large scale land surface modeling are flow velocity error, cross-section error, flow direction error and low spatial–temporal resolution, if we assume that input data (runoff) of the model are of absolute correctness. Flow velocity is spatially variable and related to topography gradient and the hydraulic radius (Arora *et al*. 1999; Arora & Boer 1999, 2001; Arora 2001). In land surface modeling, flow velocity is often treated as a constant (Oki *et al.* 2001; Nohara *et al.* 2006). Cross section also receives simple treatment and is often assumed to be rectangular in open channels (Keskin *et al.* 1997; Paiva *et al.* 2011). With advent of GIS technology and DEMs, more realistic treatments of flow velocity and cross sections can be implemented (Goteti *et al.* 2008).

Basin boundaries are irregular because of natural topographic formations. LSMs are usually run over low resolution spatial rectangular grids, leading to mismatch of natural and model defined basin boundaries and resulting in routing errors. Gong *et al.* (2009) showed that finer spatial resolution enhances routing simulation efficiency. Errors in river networks are another source of errors in streamflow routing. Davies & Bell (2009) compared four different methods for deriving river networks and showed that the routing errors from low-resolution river networks are larger than that from high-resolution river networks.

Determining flow direction for each grid cell is very important in correctly routing streamflow discharge. Shaw *et al.* (2005) proposed an automated method to determine flow direction using flow vectors. Renssen & Knoop (2000) constructed a global $0.5^\circ \times 0.5^\circ$ river routing network based on DEM and on information on major river locations.

RTM in CLM3.5 is a grid based routing model that treats routing as a linear reservoir process, i.e., the amount of streamflow from each grid cell is linearly proportional to the total runoff generated in the cell. The default grid cell size of RTM is $0.5^\circ \times 0.5$. Flow direction in each grid cell is determined by the D-8 method, i.e., water may flow in eight possible directions. The flow velocity is set as a global constant. The simplifications made by RTM in the routing scheme can lead to poor streamflow routing performance by CLM. In this study, we present the catchment-based kinematic wave routing (KWR) scheme to simulate the movement of water through floodplains and river channels. KWR can be coupled with CLM, which is still run on grids, but the routing model is set to run over catchments. KWR was tested in nine major river basins in China. We performed a comparison between the simulated streamflow results from RTM and KWR. For the remainder of this paper, we briefly describe RTM and KWR. The data sets used in this study are described, followed by the evaluation results using the new KWR model and finally conclusions and discussions are provided.

MODEL DESCRIPTION

River transport model in CLM

The RTM (Oleson *et al.* 2010) uses a linear transport scheme at 0.5° resolution to route water from each grid cell to its downstream neighboring grid cell. Flow direction in each grid cell is determined by the D-8 method. It is assumed that each grid is a reservoir. Water from one cell to its downstream neighboring cell is calculated by considering water balance of inflows and outflows (Dai & Trenberth 2002):

$$\frac{ds}{dt} = \sum F_{\text{in}} - F_{\text{out}} + R \tag{1}$$

$$F_{\text{out}} = \frac{v}{d} S \tag{2}$$

where $\sum F_{\text{in}}$ is the sum of water inflows from all neighboring upstream grid cells ($m^3\ s^{-1}$), F_{out} is the flux of water leaving the grid cell in the downstream direction ($m^3\ s^{-1}$), R is the total runoff generated in the grid cell by the land model ($m^3\ s^{-1}$), v is the effective water flow velocity ($m^3\ s^{-1}$), d is the distance between centers of neighboring grid cells (m), and s is the volume of river water stored within the grid cell (m^3). The effective water flow velocity is a global constant and is set to $0.35\ m^3\ s^{-1}$.

The total runoff from the land model at each time step is:

$$R = q_{\text{over}} + q_{\text{drai}} + q_{\text{rgwl}} \tag{3}$$

where q_{over} is surface runoff, q_{drai} is sub-surface drainage, and q_{rgwl} is liquid runoff from glaciers, wetlands, and lakes (all in $kg\ m^{-2}\ s^{-1}$).

Catchment-based kinematic wave routing scheme

In this sub-section we present a new, catchment based KWR model as an alternative to RTM to be coupled with CLM. Kinematic wave simplifies the full de Saint Venant equation, in which the friction term in the momentum equation is ignored. It thus assumes that the friction and gravity forces balance each other (Singh 1996). Assuming that friction slope (S_f) is equal to river bed slope (S_0) and river flow is gradually varied unsteady flow in open channels (Ye *et al.* 2006), we can write the continuity equation as:

$$\frac{\partial A}{\partial t} + \frac{\partial Q}{\partial x} = q \tag{4}$$

where A is river cross-sectional area (m^2), t is time(s), Q is discharge (m^3 s^{-1}), x is flow path (m), and q is lateral inflow (m^3 s^{-1}).

While CLM is generally run based on a rectangular gridded structure (typically $0.5^\circ \times 0.5^\circ$ spatial resolution), KWR is designed to run over a catchment. Catchment routing has several advantages over routing over grids. First, it can overcome the routing errors due to the mismatch of boundary between grid and catchment. Second, flow direction is more accurate over a catchment than a grid, since water always flows along the river stream within the catchment. Third, there are several possible different flow directions in a large grid, but only one direction is possible within a catchment (see Figure 1).

In RTM, total runoff in each grid is accumulated at each time step and sub-basins replace grids as routing units. If the area of grid is approximately the same as the sub-basin, sub-basin runoff is equal to grid runoff. If there is a big area difference between grid and sub-basin, it is necessary to downscale big grids to smaller grids, then accumulate runoff from all small contributing grids to sub-basin runoff (see Figure 2).

Equation (4) applies to both slope (grid) routing over sub-basins (grids) and river channel routing. Because of the different representations of cross section for slopes and river channels, Equation (4) is solved differently. Below shows how Equation (4) is solved for slopes and river channels.

Slope routing in a sub-basin

A rectangular cross section is usually assumed in slope routing (Keskin *et al.* 1997), in which water depth (h) is equal to water section area divided by river length (see Figure 3):

$$h = \frac{A}{w} \tag{5}$$

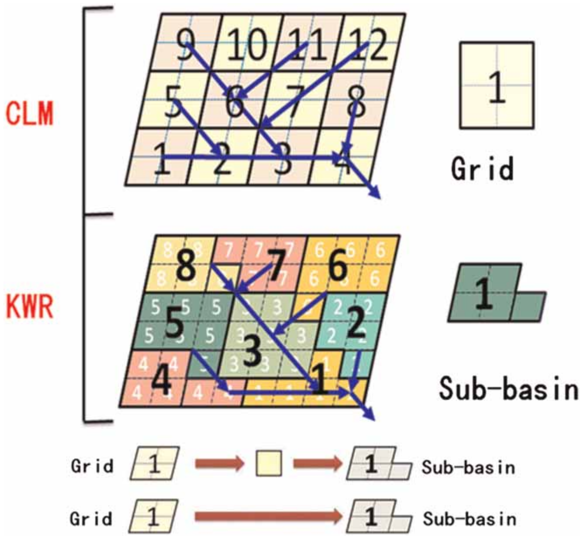

Figure 2 | Mapping CLM grids to sub-basins used by KWR.

where A is water flow cross-sectional area (m^2), and w is water flow cross-sectional width (m).

Flow velocity (v, m s^{-1}) is calculated based on Manning's formula (Arora & Boer 1999):

$$v = \frac{1}{n} \cdot R_a^{\frac{2}{3}} S_0^{\frac{1}{2}} = \frac{1}{n} \cdot \left(\frac{A}{w+2h}\right)^{\frac{2}{3}} S_0^{\frac{1}{2}} = \frac{1}{n} \cdot \left(\frac{Aw}{w^2+2A}\right)^{\frac{2}{3}} S_0^{\frac{1}{2}} \tag{6}$$

where n is Manning roughness coefficient, S_0 is the river bed slope, and R_a is the hydraulic radius.

The discharge at river cross section is computed as:

$$Q = A \cdot v \tag{7}$$

We assume that river path is in the middle of two slopes in a sub-basin, and the cross-sectional width w is equal to the river length L, $w = L$ (m) (see Figure 3). The discharge from

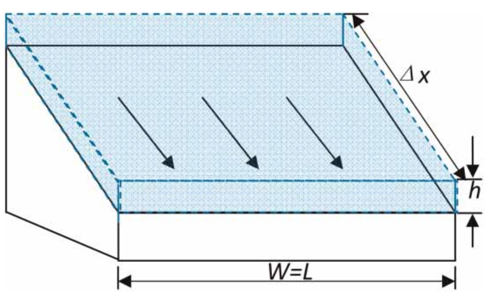

Figure 3 | Schematic illustration of slope.

the cross-section can be computed as:

$$Q = A\cdot v = A\cdot\frac{1}{n}\left(\frac{Aw}{w^2+2A}\right)^{\frac{2}{3}}S_0^{\frac{1}{2}} = A\cdot\frac{1}{n}\left(\frac{AL}{L^2+2A}\right)^{\frac{2}{3}}S_0^{\frac{1}{2}}$$
$$= \frac{1}{n}S_0^{\frac{1}{2}}\cdot\left(\frac{A^{\frac{5}{2}}L}{L^2+2A}\right)^{\frac{2}{3}} = \alpha\cdot\left(\frac{A^{\frac{5}{2}}L}{L^2+2A}\right)^{\frac{2}{3}} \tag{8}$$

where $\alpha = \frac{1}{n}S_0^{\frac{1}{2}}$. Equation (4) can be represented by a finite difference approximation:

$$\frac{\Delta A}{\Delta t} + \frac{\Delta Q}{\Delta x} = q \rightarrow \Delta A\Delta x + \Delta Q\Delta t = q\Delta x\Delta t \tag{9}$$

If we assume that river path is in the middle of two slopes, then average flow path length (Δx) over the slope can be calculated by:

$$\Delta x = \frac{\text{Area}}{2L} \tag{10}$$

where Area is the sub-basin area. Given that the lateral inflow term q is equal to runoff (R) from the sub-basin, then Equation (9) can be written as:

$$\Delta A\Delta x + \Delta Q\Delta t = R\cdot\frac{\text{Area}}{2} \tag{11}$$

Denoting $\Delta A = A_t - A_{t-1}$ at t time and $\Delta Q = Q_s$, where Q_s is discharge ($m^3\ s^{-1}$) from the slope to river of half sub-basin, and Q_s can be calculated by the following expression:

$$Q_s = \alpha\cdot\left[\frac{\left(\frac{A_t+A_{t-1}}{2}\right)^{\frac{5}{2}}L}{L^2+2\left(\frac{A_t+A_{t-1}}{2}\right)}\right]^{\frac{2}{3}}$$
$$= 2^{-\frac{5}{3}}\alpha\cdot\left[\frac{(A_t+A_{t-1})^{\frac{5}{2}}L}{L^2+(A_t+A_{t-1})}\right]^{\frac{2}{3}} \tag{12}$$

Combining Equations (10) and (12) with (11), we obtain:

$$(A_t - A_{t-1}) = \left(-2^{-\frac{5}{3}}\alpha\cdot\left[\frac{(A_t+A_{t-1})^{\frac{5}{2}}L}{L^2+(A_t+A_{t-1})}\right]^{\frac{2}{3}}\right)\frac{\Delta t}{\Delta x}$$
$$+ R\cdot\frac{\text{Area}}{\Delta x} \tag{13}$$

If we set $P = -2^{-\frac{5}{3}}\alpha\frac{\Delta t}{\Delta x}$ and $Q = A_t + A_{t-1}$, then we obtain:

$$f(A_t) = \left(-2^{-\frac{5}{3}}\alpha\cdot\left[\frac{(A_t+A_{t-1})^{\frac{5}{2}}L}{L^2+(A_t+A_{t-1})}\right]^{\frac{2}{3}}\right)\frac{\Delta t}{\Delta x} + R\cdot\frac{\text{Area}}{\Delta x}$$
$$- A_t + A_{t-1} = P\left[\frac{Q^{\frac{5}{2}}L}{L^2+Q}\right]^{\frac{2}{3}} + R\cdot\frac{\text{Area}}{\Delta x} - A_t + A_{t-1} \tag{14}$$

and

$$f'(A_t) = \left(\frac{2}{3}\cdot P\left[\frac{Q^{\frac{5}{2}}L}{L^2+Q}\right]^{-\frac{1}{3}}\cdot\left[\frac{5}{2}\frac{Q^{\frac{3}{2}}L}{L^2+Q} - Q^{\frac{5}{2}}L\right] - 1\right)$$
$$= \left(-\frac{2}{3}\cdot 2^{-\frac{5}{3}}\alpha\frac{\Delta t}{\Delta x}\left[\frac{(A_t+A_{t-1})^{\frac{5}{2}}L}{L^2+(A_t+A_{t-1})}\right]^{-\frac{1}{3}}\right)$$
$$\cdot\left[\frac{5}{2}\frac{(A_t+A_{t-1})^{\frac{3}{2}}L}{L^2+(A_t+A_{t-1})} - (A_t+A_{t-1})^{\frac{5}{2}}L\right] - 1 \tag{15}$$

With Newton iterations:

$$A_t^{(k)} = A_t^{(k-1)} - \frac{f(A_t^{(k-1)})}{f'(A_t^{(k-1)})} \tag{16}$$

we can first obtain water flow cross-sectional area, and then use Equation (12) to calculate the discharge ($m^3\ s^{-1}$) from slope to river.

River routing in a sub-basin

Some of the river routing equations are exactly the same as those of slope routing, e.g., average water depth (h, m), flow velocity (v, m s^{-1}), and discharge at the river cross section Q_s.

Along the river path in a sub-basin, average width of cross section changes with water depth (see Figure 4). It is assumed that cross section is a triangle which angles are constant, and then the cross-sectional average width and

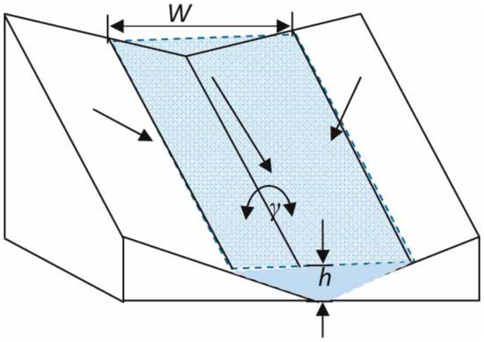

Figure 4 | Schematic illustration of a river channel.

water depth are linearly dependent (Coe *et al.* 2008; Paiva *et al.* 2011):

$$a = \tan\frac{\gamma}{2} = \frac{w/2}{h} \rightarrow w = 2a \cdot h \tag{17}$$

where h is average depth(m), w is average width(m), a is a parameter which is determined by river attribute, γ is the included angle of two riversides, tan is trigonometric function.

Assuming a triangle cross section in river routing, we obtain:

$$A = \frac{h \cdot w}{2} \rightarrow h = \frac{2A}{w} = \frac{A}{ah} \rightarrow h = \left(\frac{A}{a}\right)^{\frac{1}{2}} \tag{18}$$

Combining Equations (6) and (18), we obtain:

$$\begin{aligned} v &= \frac{1}{n} \cdot R_a^{\frac{2}{3}} S_0^{\frac{1}{2}} = \frac{1}{n} \cdot \left(\frac{A}{w+2h}\right)^{\frac{2}{3}} S_0^{\frac{1}{2}} \\ &= \frac{1}{n} \cdot \left(\frac{A}{ah+2h}\right)^{\frac{2}{3}} S_0^{\frac{1}{2}} = \frac{1}{n} S_0^{\frac{1}{2}} \cdot \left(\frac{(aA)^{\frac{1}{2}}}{a+2}\right)^{\frac{2}{3}} \\ &= \frac{1}{n} S_0^{\frac{1}{2}} (a+2)^{-\frac{2}{3}} \cdot a^{\frac{1}{3}} \cdot A^{\frac{1}{3}} \end{aligned} \tag{19}$$

Combining Equations (7) and (19), we obtain:

$$\begin{aligned} Q &= A \cdot v = A \cdot \frac{1}{n} S_0^{\frac{1}{2}} (a+2)^{-\frac{2}{3}} \cdot a^{\frac{1}{3}} \cdot A^{\frac{1}{3}} \\ &= \frac{1}{n} S_0^{\frac{1}{2}} (a+2)^{-\frac{2}{3}} \cdot a^{\frac{1}{3}} \cdot A^{\frac{4}{3}} = \alpha \cdot A^{\beta} \end{aligned} \tag{20}$$

By setting $\alpha = \frac{1}{n} S_0^{1/2} (a+2)^{-2/3} \cdot a^{1/3}$, $\beta = 4/3$ flow route length (Δx) equal to the river length: $\Delta x = \mathrm{L}$, inflow term q equal to lateral flow term $2Q_s$, the finite difference representation of Equation (4) is:

$$\Delta AL + \Delta Q \Delta t = 2Q_s \Delta t \tag{21}$$

Denoting $\Delta A = A_t - A_{t-1}$ at t time and $\Delta Q = Q_O - Q_I$, where A is water flow cross-sectional area (m^2), Q_I is input discharge ($m^3\,s^{-1}$), Q_O is output discharge ($m^3\,s^{-1}$), the output discharge is:

$$Q_O = \alpha \cdot \left(\frac{A_t + A_{t-1}}{2}\right)^{\beta} \tag{22}$$

Combining Equations (20) and (21) with (22), we obtain:

$$(A_t - A_{t-1}) = \left(Q_I - \alpha \cdot \left(\frac{A_t + A_{t-1}}{2}\right)^{\beta}\right) \frac{\Delta t}{L} + \frac{Q_s \Delta t}{L} \tag{23}$$

If we set

$$f(A_t) = \left(Q_I - \alpha \cdot \left(\frac{A_t + A_{t-1}}{2}\right)^{\beta}\right) \frac{\Delta t}{L} + \frac{Q_s \Delta t}{L} - A_t + A_{t-1} \tag{24}$$

$$f'(A_t) = -\frac{\alpha\beta}{2} \cdot \left(\frac{A_t + A_{t-1}}{2}\right)^{\beta-1} \frac{\Delta t}{L} - 1 \tag{25}$$

$$A_t^{(k)} = A_t^{(k-1)} - \frac{f(A_t^{(k-1)})}{f'(A_t^{(k-1)})} \tag{26}$$

we can obtain water flow cross-sectional area and river output discharge ($m^3\,s^{-1}$) with Equation (22).

Routing between sub-basins

Using ArcGis software or an automatic drainage network extraction method (Ye *et al.* 2005), we define a flow direction and a serial number for each sub-basin. The whole domain is a directed, but non-loop graph based on sub-basins (see Figure 1). The upstream sub-basin number always is larger than the downstream sub-basin number.

The river stream network is encoded from the outlet of the basin to upstream (Figure 5) (Ye *et al.* 2005). The routing is calculated from upstream to downstream, and ultimately to the basin outlet, i.e., it calculates from the sub-basin with largest index number to the basin outlet which is indexed sub-basin number 1.

DATA USED IN THIS STUDY

CLM requires basic climate forcing data as inputs. We used the global atmospheric forcing data developed by Sheffield *et al.* (2006). This dataset contains precipitation, surface temperature, pressure, and humidity, wind speed and incoming short- and long-wave radiation, available at a spatial resolution of 1.875° and a temporal resolution of 3 h. Land surface information data are adopted from the IGBP (International Geosphere-Biosphere Programme) Global 1 km Land Cover Data Set. The forcing data and land surface data are interpolated into grids at 0.5° horizontal resolution. The observed daily discharge data from nine major river basins in China, which were transformed from stage measurements, were obtained for this study (see Tables 1 and 2). The study domain is the entire continental China (located 89.5–134.5°E, 17.5–54.5°N; Figure 6). Runoff simulated by CLM in the 1995–2004 period were used as the input data to drive RTM and KRM. RTM is run on a 0.5° × 0.5° grid (Figure 7). KWR is run over 37,992 sub-basins, with a minimum sub-basin area of >100 km^2 (Figure 8). The location of the streamflow discharge gauge stations are shown in Figure 9.

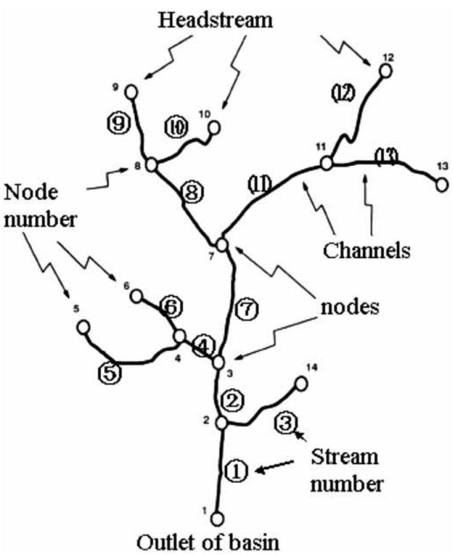

Figure 5 | Schematic illustration of stream networks.

MODEL EVALUATION

Analysis of the routing results

Using the aforementioned atmospheric forcing data and land cover data to drive CLM, we obtained daily grid-based runoff at 0.5° resolution. Figure 10 shows the annual simulated runoff from CLM in 2003 and 2004. The daily grid-based runoff was mapped into catchments. The simulated runoff outputs are then used to drive RTM and KWR, respectively. Figure 11 shows that the spatial resolution of KWR is finer than that of RTM. The flow direction of KWR appears more realistic compared to that of RTM. The simulated discharge of KWR is concentrated in river channels. Because RTM is run on 0.5° × 0.5° grid, the river channel width of RTM is equal to 50 km, which is much greater than in reality. Further, a close inspection of the flow

Table 1 | Nine basin regions attributes in China

Basin name	Sub-basin number	Sub-basin quantity	Average elevation/m	Basin area/ 10,000 km^2
Yangtze	1–7,300	7,300	1,624	179.8269
Yellow	7,301–10,601	3,301	1,896	80.6620
Huai	10,602–11,909	1,308	87	32.5151
Hai	11,910–13,182	1,273	592	31.6429
Songliao	13,183–18,199	5,017	445	123.3228
Pear	18,200–20,437	2,238	517	56.7777
South–West	20,438–23,805	3,368	3,762	84.8405
South–East	23,806–24,642	837	478	23.5292
Inland	24,643–37,992	13,350	2,563	333.6037

Table 2 | Streamflow stations attributes

Station	Basin	Sub-basin NO.	Accumulative upslope area	Longitude	Latitude	Observed streamflow
Datong	Yangze River	291	1,703,156	117.61	30.78	2002–2004
Sanshui + Makou	Pear River	18,215	39,2721	112.83	23.17	2001–2203
Jiamusi	Songhuajiang River	14,157	527,971	100.15	35.50	1995–1998
Liujianfang	LiaoHe River	13,868	144,960	122.53	41.29	1996–2004
Xiaoliuxiang	Huaihe River	11,270	132,768	118.13	33.17	2001–2004
Tangnaihai	Yellow River	10,068	123,387	130.37	46.82	1995–1997
Huayuankou	Yellow River	7,379	776,190	113.67	34.91	1997–1999

Figure 6 | Nine major river basins in China.

direction of RTM indicates that they are not realistic either.

Table 3 shows the performance statistics of the simulated discharge by both RTM and KWR as compared to the observations at the gauge stations of the nine river basins. The performance measures include the Nash–Sutcliffe efficiency (NSE) value E; correlation coefficient R; and water balance coefficient B. They are computed as follows:

$$E = \left[1 - \frac{\sum (Q_C - Q_O)^2}{\sum (Q_O - \overline{Q_O})^2}\right] \times 100\% \tag{27}$$

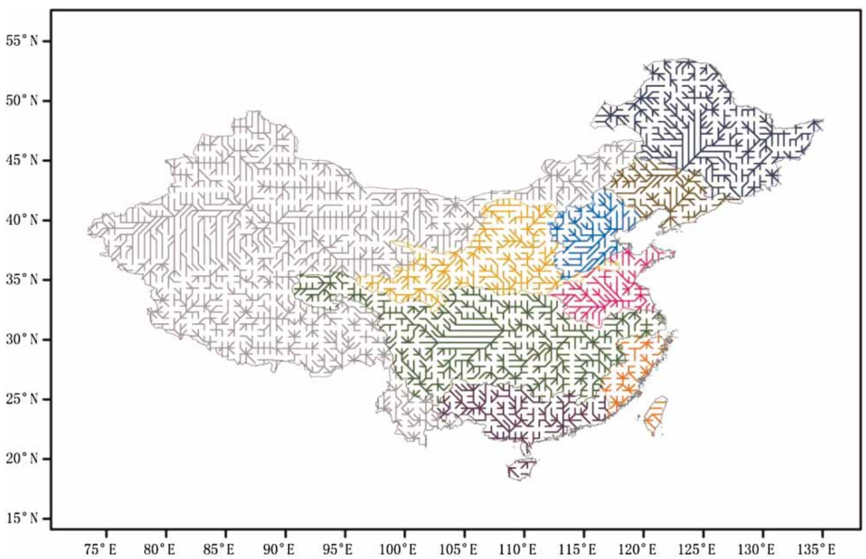

Figure 7 | RTM grid flow direction in continental China (0.5° by 0.5° grid).

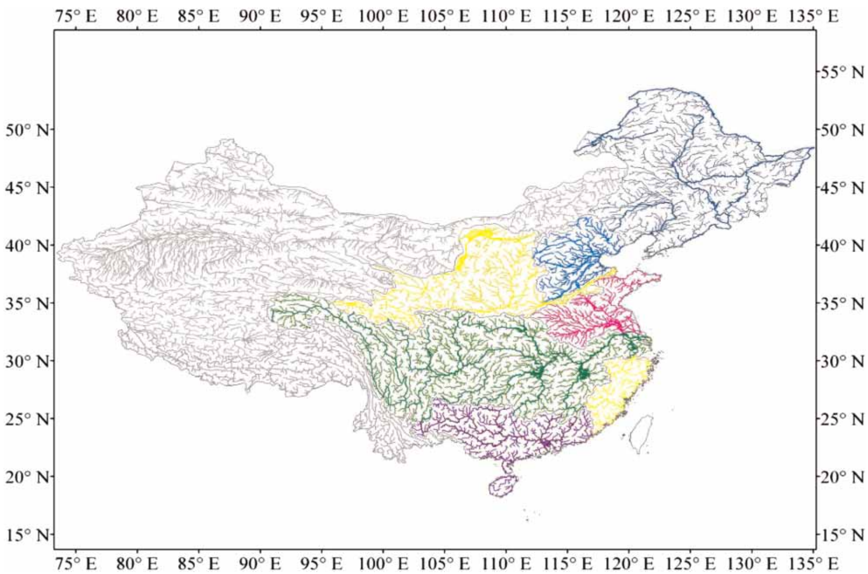

Figure 8 | KWR river network in continental China (100 km^2 sub-basin).

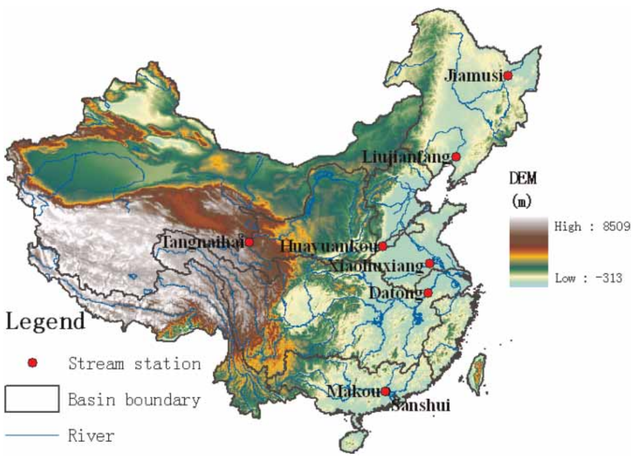

Figure 9 | Elevation map and streamflow gauge station location.

$$R = \frac{\sum (Q_c - \overline{Q}_c)(Q_o - \overline{Q}_o)}{\sqrt{\sum (Q_c - \overline{Q}_c)^2 \sum (Q_o - \overline{Q}_o)^2}} \tag{28}$$

$$B = \frac{SR}{OR} \tag{29}$$

where $Q_O, Q_C, \overline{Q_o}, \overline{Q_c}$ are observed discharge, simulated discharge, average observed discharge and average simulated discharge, respectively; SR is the sum of simulated discharge, and OR is the sum of observed discharge. For E and R, the bigger the values are, the better the model performance. The perfect value for both measures is

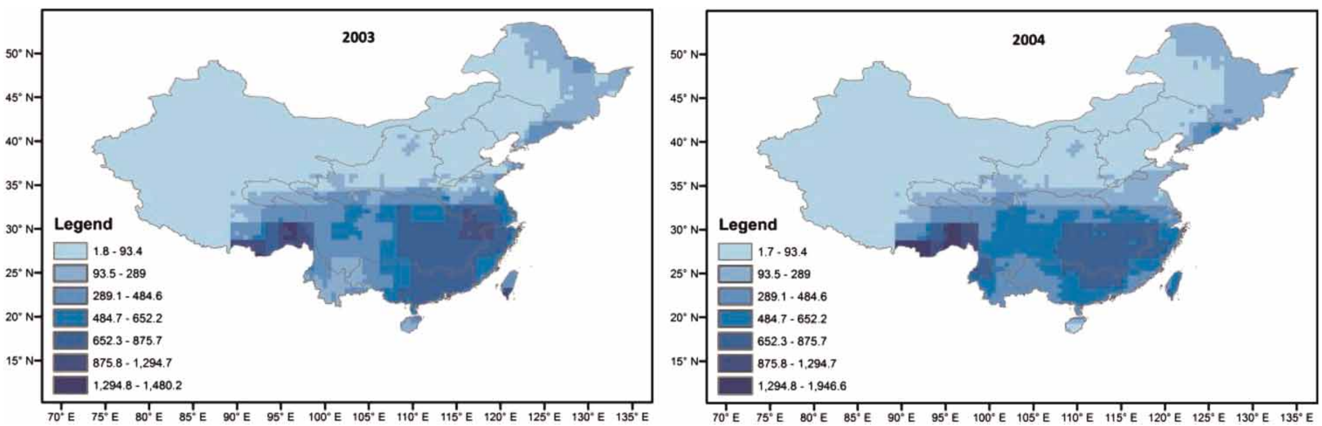

Figure 10 | Simulated annual runoff by CLM in 2003 and 2004.

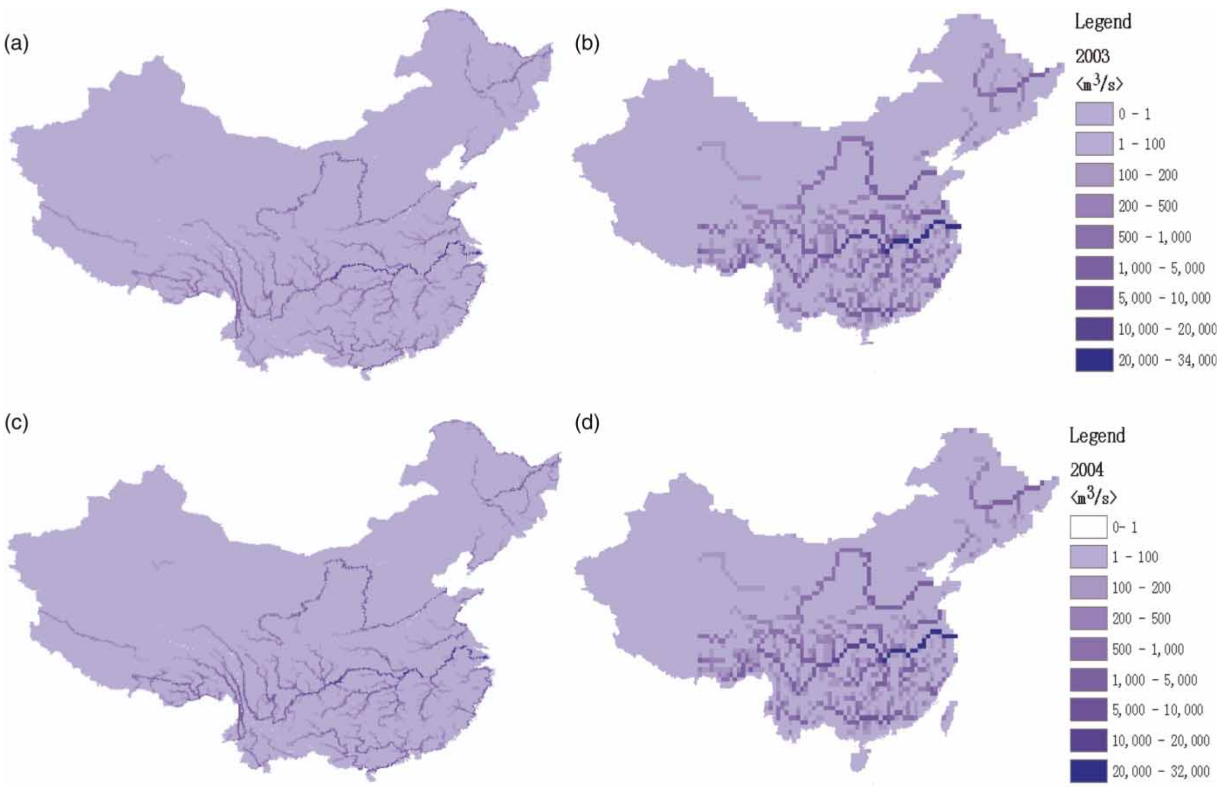

Figure 11 | Simulated annual discharge by KWR and RTM in 2003 and 2004. (a) discharge in 2003 by KWR, (b) discharge in 2003 by RTM, (c) discharge in 2004 by KWR, (d) discharge in 2004 by RTM.

Table 3 | Simulated discharge and observed discharge comparison statistics over the gauge stations

Station	Basin	Utilization of water resources (%)	*E* KWR	*E* RTM	*R* KWR	*R* RTM	*B* KWR	*B* RTM
Datong	Yangze River	17.193	0. 79	−1.95	0. 95	0.79	1.07	1.24
Sanshui + Makou	Pear River	18.619	0.73	−1.46	0.91	0.56	1.02	1.34
Jiamusi	Songhuajiang River	44.274	0.76	0.75	0.90	0.89	1.00	0.97
Liujianfang	LiaoHe River	44.274	0.44	0.41	0.79	0.67	1.95	1.45
Xiaoliuxiang	Huaihe River	44.746	0.44	−0.20	0.78	0.54	1.56	1.87
Tangnaihai	Yellow River	69.167	0.11	−2.91	0.74	0.40	1.15	1.85
Huayuankou	Yellow River	69.167	−1.67	−0.34	0.36	0.19	1.67	0.92

Utilization of water resources is from Bulletin of Water Resources in China (2000).

equal to 1. For E, a negative value implies that the model performance is worse than the long-term average. The perfect value for B is also equal to 1. The value of less than 1 or greater than 1 means underestimation or overestimation of discharge, respectively. Table 3 also includes a measure called Utilization of water resources, which is defined as the ratio of water use and water availability (Bulletin of Water Resources in China 2000). Water availability is defined by precipitation received in the basin while water use is defined as water consumption in three major sectors in the basin: agriculture, domestic and industry. A high utilization of water resources indicates the disruption of natural flow is severe.

Based on statistics shown in Table 3, the performance statistics of KWR is generally much better that of RTM, as E and R of KWR are larger than that of RTM and B of KWR is closer to 1 than B of RTM in most cases. But there are several exceptions. For example, the statistics for the two Yellow River gauge stations indicates that KWR may perform worse than RTM. The B value of KWR for Liaohe basin is much larger compared to that of RTM. It can be noted that utilization of water resources is very high in both cases, implying that the observed discharge is highly influenced by human activities and is therefore not reliable. This also implies that it is difficult to validate streamflow discharge in basins where the influence of human activities is very strong. Figure 12 provides a visual comparison between KWR and RTM. Even though there are differences between simulated and observed discharge for both KWR and RTM, the simulated discharge by KWR is much closer to observations than that by RTM, especially in terms of flood peak timing and magnitude (Arora & Boer 1999).

Parameter sensitivity and uncertainly analysis

The results from the previous section indicate that KWR outperforms RTM in simulating streamflow discharge in most cases. Two questions are raised: (1) how to quantify the uncertainty of using a rating curve to transform stage measurements into discharge estimates (observed discharge); and (2) how to quantify the uncertainty in the estimates of streamflow discharge (simulated discharge) by KWR. The main sources of uncertainty in observed discharge estimates are cross-section state, gauging measurements and the rating curve (McMillan *et al.* 2010). There are several sources of uncertainty in the simulated streamflow discharge estimates: the runoff generated by CLM, the initial and boundary conditions and KWR model errors. For this study, the uncertainty due to initial conditions is ignored because their effects can be reduced by using an adequate warm-up period. We will not address the uncertainty due to the runoff generated by CLM as it is beyond the scope of this paper. We focus on the uncertainty from the KWR model error and observed discharge error (i.e., the uncertainty due to the specification of KWR parameters and the stage–discharge rating curve parameters). We only analyze uncertainty in discharge observations and simulations of three rivers: Yangtze, Pearl and Songhuajiang because utilization of water resources in these basins is relatively small.

The flexible and widely used power law equation was chosen to fit stage–discharge rating curve (Pappenberger *et al.* 2006; Krueger *et al.* 2009, 2010; Yanli *et al.* 2009; McMillan *et al.* 2010; Westerberg *et al.* 2011):

$$Q = \lambda \cdot (H - b)^c \quad \begin{cases} b = 0 & if \quad H_b \leq 0 \\ b = H_b & if \quad H_b > 0 \end{cases} \tag{30}$$

where Q is discharge ($m^3\ s^{-1}$), h is stage height (m), and λ, b and c are parameters which was chosen as the rating equation, H_b is river bed elevation (m). Since parameter b has some physical justification for rivers that flow into the sea, we first determine the b value from the attribute of the gauging cross-section. Parameters λ and c are the only tunable parameters in Equation (30) (see Table 4).

There are only two tunable parameters in KWR: Manning roughness coefficient (n range: 0.01–0.5) and the ratio of river width and depth (a range: 1–150) (Table 4). Both parameters are attributes of the river, and in theory, can be observed at a particular location. But in large scale land surface modeling, it is impossible to measure them at all locations.

There are many ways to perform uncertainty analysis. The Generalized Likelihood Uncertainty Estimation (GLUE) (Beven & Binley 1992) is popular with many hydrologic modelers (Liu *et al.* 2009; Krueger *et al.* 2010; Westerberg *et al.* 2011). In this study, we used the software known as 'A Problem Solving environment for Uncertainty Analysis and Design Exploration', PSUADE (Tong 2006, 2010, 2011). PSUADE has a rich set of tools for screening important model parameters, generating response surface, and performing global sensitivity analysis, design optimization, and model calibration.

We choose a quasi-random sequence sampling method (i.e., LP-τ) (Sobol' *et al.* 1992) to create 1,000 (10,000 for stage–discharge rating curve) samples in the feasible

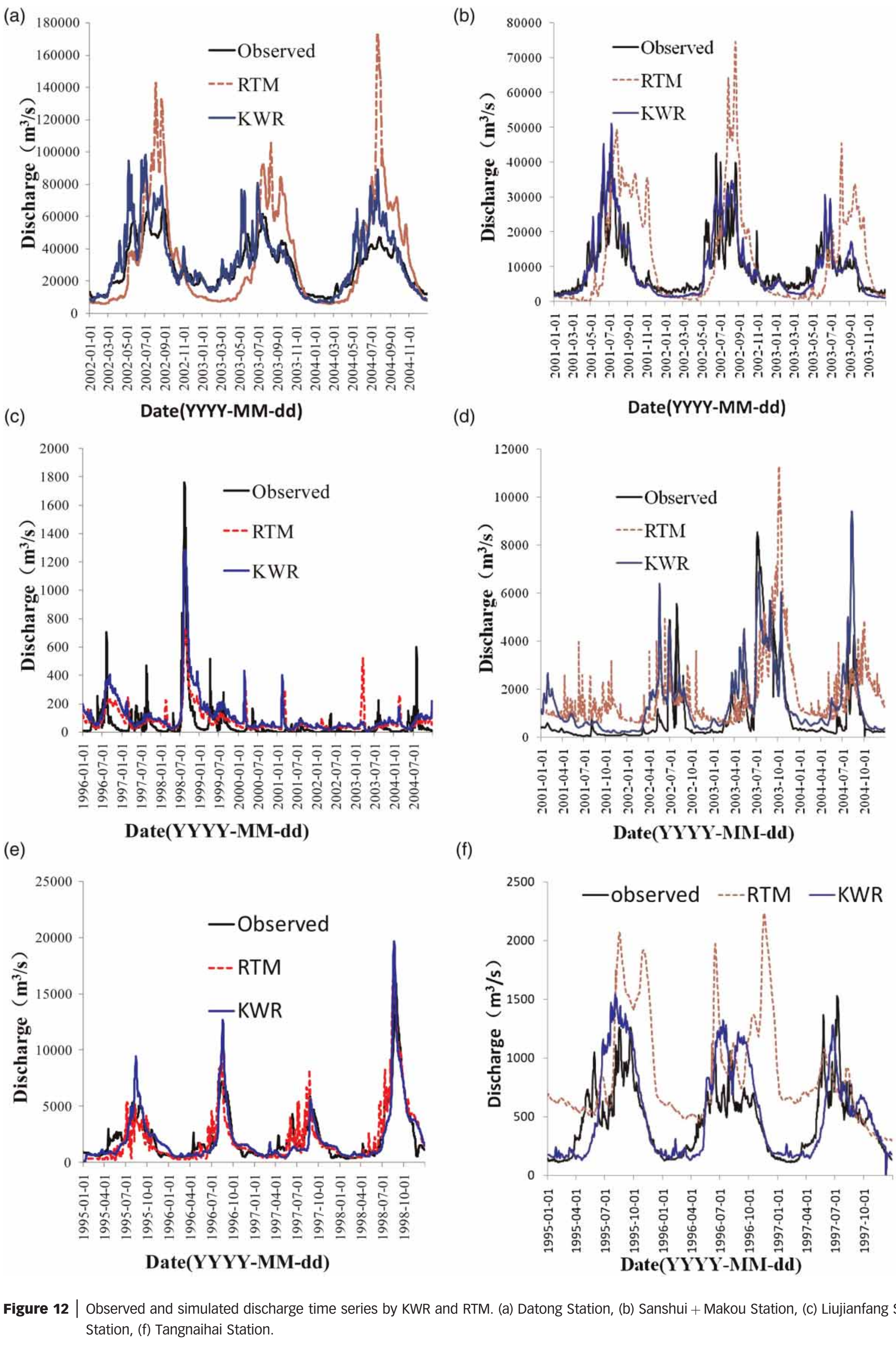

Figure 12 | Observed and simulated discharge time series by KWR and RTM. (a) Datong Station, (b) Sanshui + Makou Station, (c) Liujianfang Station, (d) Xiaoliuxiang Station, (e) Jiamusi Station, (f) Tangnaihai Station.

Table 4 | Parameters of stage–discharge rating curves and KWR

Basin	Parameter	Optimal value	Sampling range	Samples
Yangtze	λ	1,033	1,000–1,200	756 ($E > 0.9$)
	c	1.5	1–2.5	
	b	0		
	n	0.3	0.01–0.5	1,000
	a	110	1–150	
Pearl (Sanshui/Makou)	λ	1,500/4,058	1,000–2,000/3,500–5,000	1,437/1,759 ($E > 0.9$)
	c	1.1/1.1	0.7–2/0.7–2	
	b	0.11/0.45		
	n	0.3	0.01–0.5	1,000
	a	110	1–150	
Songhuajiang	λ	161	100–500	1,044 ($E > 0.9$)
	c	1.9	1–2	
	b	71		
	n	0.15	0.01–0.5	1,000
	a	60	1–150	

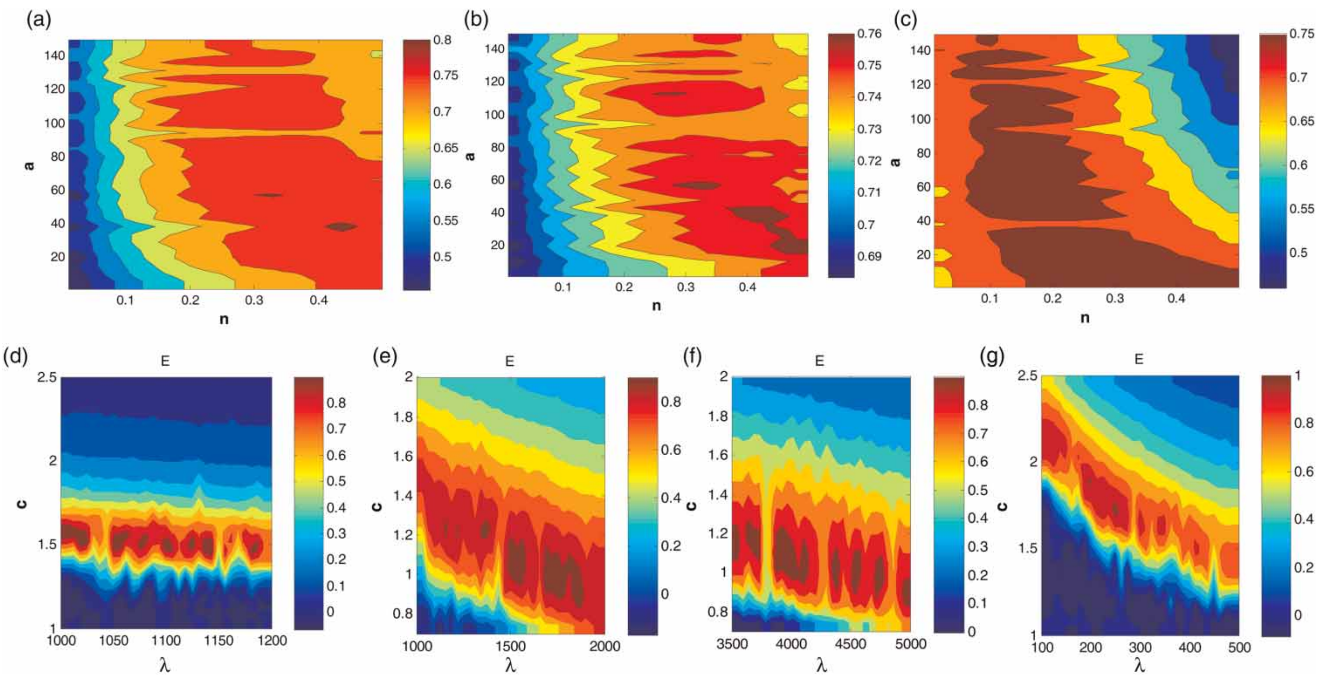

Figure 13 | Response surfaces of KWR model parameters. (a) Yangtze (n, a), (b) Pearl (n, a), (c) Songhuajiang (n, a), (d) Yangtze (λ, c), (e) Pearl (Sanshui) (λ, c), (f) Pearl (Makou) (λ, c), (g) Songhuajiang (λ, c).

parameter space. Using the 1,000 (10,000) samples, we create a response surface based on a goodness of fit measure between simulated discharge and observed discharge at the streamflow gauge stations. The goodness of fit measure used is the NSE as defined in Equation (27). Figure 13 shows the response surfaces for Yangtze, Pearl and Songhuajiang rivers. Figure 14 shows the NSE values projected on to the axes of the four parameters. It can be seen from both figures that the response surfaces are behaved reasonably. The NSE value varies smoothly with Manning's n and parameter c in the feasible range. For different rivers, the optima of parameters are located at different values (Table 4). On the

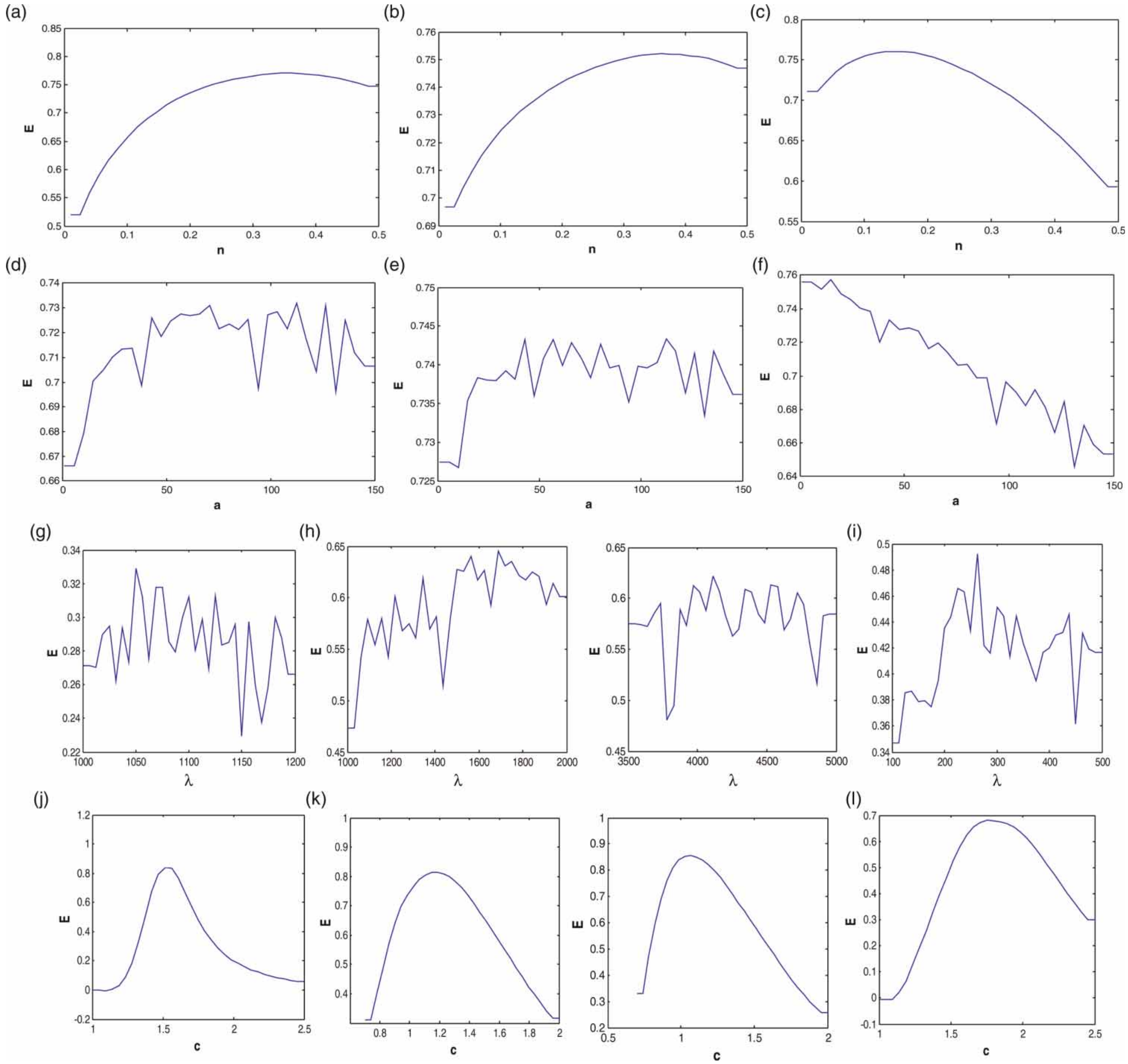

Figure 14 | The NSE values projected on to the axes of parameters. (a) Yangtze (*n*), (b) Pearl (*n*), (c) Songhuajiang (*n*), (d) Yangtze (*a*), (e) Pearl (*a*), (f) Songhuajiang (*a*), (g) Yangtze (λ), (h) Pearl (Sanshui & Makou) (λ), (i) Songhuajiang (λ), (j) Yangtze (*c*), (k) Pearl (Sanshui & Makou) (*c*), (l) Songhuajiang (*c*).

other hand, the relationship between NSE and cross section depth-to-width ratio, *a*, is not as smooth and exact optimal values are difficult to identify. The relationship between NSE and parameter λ is also similar.

Based on these response surfaces, we run a Monte-Carlo Markov Chain (MCMC) search algorithm to find the posterior probability distribution functions (PDFs) of the parameters. Figure 15 shows the posterior PDFs of parameter *n* and *a* for the three basins. Parameter *n* is a sensitive parameter, as we can clearly see the peaks of the PDFs. The optimal value of *n* is about 0.3 in the Yangtze River and Pearl River, and around 0.15 in the Songhuajiang River. Parameter *a* is not as sensitive, but we can identify the peaks for the Yangtze River and Songhuajiang River (see

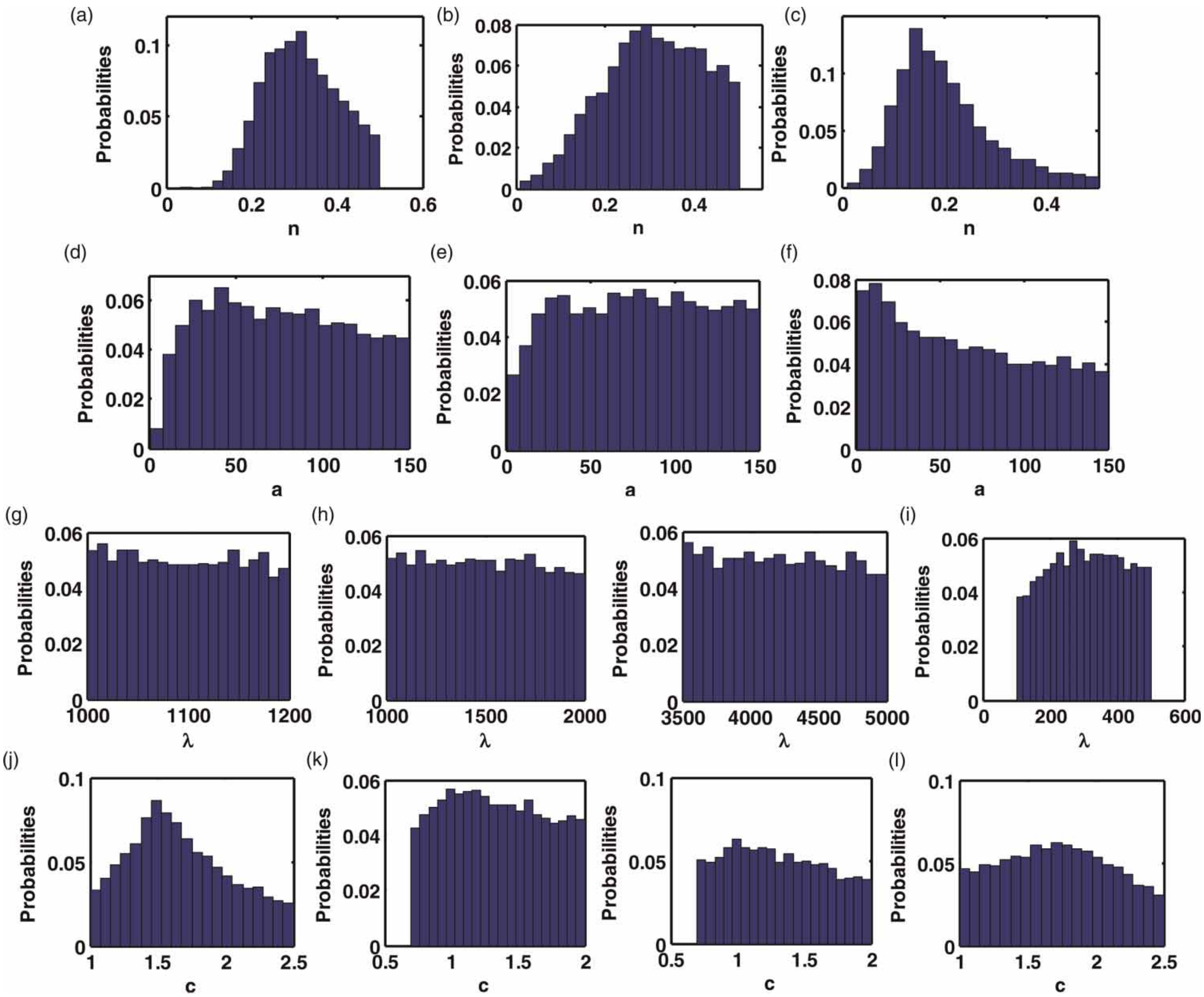

Figure 15 | The posterior PDF of parameters. (a) Yangtze (*n*), (b) Pearl (*n*), (c) Songhuajiang (*n*), (d) Yangtze (*a*), (e) Pearl (*a*), (f) Songhuajiang (*a*), (g) Yangtze (λ), (h) Pearl (Sanshui & Makou) (λ), (i) Songhuajiang (λ), (j) Yangtze (*c*), (k) Pearl (Sanshui & Makou) (*c*), (l) Songhuajiang (*c*).

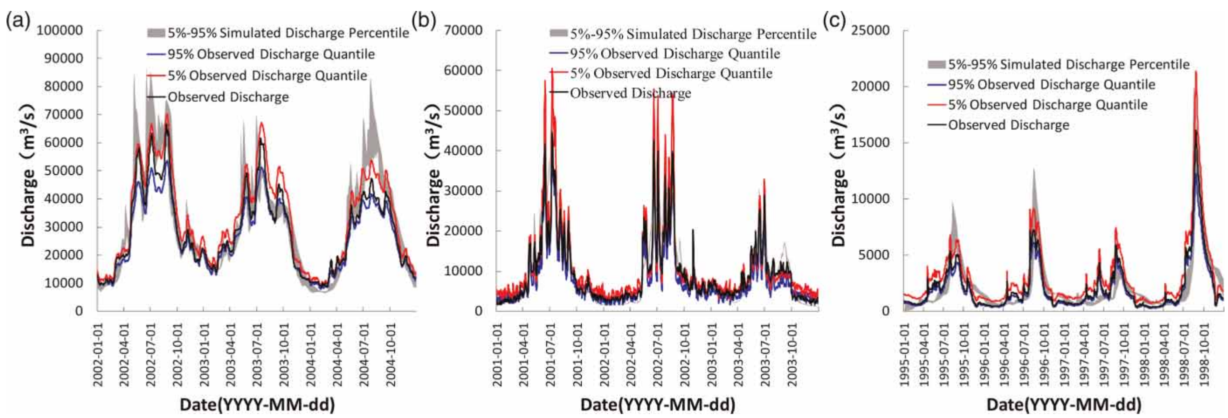

Figure 16 | Observed discharge and uncertainty range of simulated discharge. (a) Yangtze River, (b) Pearl River, (c) Songhuajiang River.

Figure 15(d) and 15(f)). For the Pearl River basin, it is difficult to identify the most likely parameter (see Figure 15(e)).

Using the final converged about 1,000 parameter sets from the MCMC search, we made 1,000 discharge simulations and obtained the 5 and 95% discharge quantiles to represent uncertainty from KWR parameters and the stage–discharge rating curve parameters for the three rivers. The 5–95 percentile quantile of observed discharge as well as the 5–95 percentile uncertainty range of the simulated discharge are plotted in Figure 16. It can be noted that the uncertainty range due to variation of parameters is relatively small, especially for the Pearl River (see Figure 16(b)). The results suggest that uncertainty in discharge routing simulated by KWR is mostly due to the uncertainty in the runoff simulation by CLM, not the parameters. The fact that KWR can provide reasonable simulation of flood timing and magnitude suggest that KWR can be a good alternative to RTM in CLM.

CONCLUSIONS AND DISCUSSION

We developed a catchment-based KWR scheme model as an alternative to the RTM model currently used in CLM3.5. The experimental results show that the KWR generally performs better than RTM when compared to observed discharge in several large river basins in China. The major differences between KWR and RTM are threefold: (1) KWR is based on the kinematic wave formulation while RTM is based on linear reservoir concept; (2) KWR uses sub-basins as routing units while RTM uses grid-based routing; and (3) KWR has a more realistic treatment of flow velocity that is based on local topography and other information. The uncertainty analysis suggests that the key source of uncertainty in discharge simulation is due to runoff simulation by CLM, while the uncertainty due to parameters of the routing model KWR is relatively minor.

The simulation results in Huaihe River and Yellow River basins are not as consistent with observations as in other river basins because intense human activities interrupt natural streamflow in these basins. However, current CLM or most other LSMs do not consider how human activities influence streamflow, which may lead to unrealistic simulated discharge inflow into the oceans. It would be an interesting follow-up study as to how this would influence the climate simulations.

ACKNOWLEDGEMENTS

This study was supported by the National Basic Research Program of China (the 973 Program: No. 2010CB428402 and No. 2010CB428403) and the Open Foundation of the Changjiang River Scientific Research Institute (CKWV2012324/KY). We would like to thank two anonymous reviewers, Associate Editor, and the Editor-in-Chief for their helpful comments which improved the article significantly.

REFERENCES

Arora, V. K. 2001 Streamflow simulations for continental-scale river basins in a global atmospheric general circulation model. *Advances in Water Resources* **24**, 775–791.

Arora, V. K. & Boer, G. J. 1999 A variable velocity flow routing algorithm for GCMs. *Journal of Geophysical Research* **104** (D24), 30965–30979.

Arora, V. K. & Boer, G. J. 2001 Effects of simulated climate change on the hydrology of major river basins. *Journal of Geophysical Research* **106** (D4), 3335–3348.

Arora, V. K., Chiew, F. H. S. & Grayson, R. B. 1999 A river flow routing scheme for general circulation models. *Journal of Geophysical Research* **104** (D12), 14347–14357.

Bajracharya, K. & Barry, D. A. 1997 Accuracy criteria for linearised diffusion wave flood routing. *Journal of Hydrology* **195**, 200–217.

Bates, P. D. & De Roo, A. P. J. 2000 A simple raster-based model for flood inundation simulation. *Journal of Hydrology* **236**, 54–77.

Bell, V. A., Kay, A. L., Jones, R. G. & Moore, R. J. 2007 Development of a high resolution grid-based river flow model for use with regional climate model output. *Hydrology and Earth System Sciences* **11**, 532–549.

Best, M. J., Pryor, M., Clark, D. B., Rooney, G. G., Essery, R. L. H., Ménard, C. B., Edwards, J. M., Hendry, M. A., Porson, A., Gedney, N., Mercado, L. M., Sitch, S., Blyth, E., Boucher, O., Cox, P. M., Grimmond, C. S. B. & Harding, R. J. 2011 The Joint UK Land Environment Simulator (JULES), model description – Part 1: Energy and water fluxes. *Geoscientific Model Development* **4**, 677–699.

Beven, K. 1979 On the generalized kinematic routing method. *Water Resources Research* **15**, 1238–1242.

Beven, K. & Binley, A. 1992 The future of distributed models: model calibration and uncertainty prediction. *Hydrological Processes* **6**, 279–298.

Biancamaria, S., Bates, P. D., Boone, A. & Mognard, N. M. 2009 Large-scale coupled hydrologic and hydraulic modelling of the Ob river in Siberia. *Journal of Hydrology* **379**, 136–150.

Birkhead, A. L. & James, C. S. 1998 Synthesis of rating curves from local stage and remote discharge monitoring using nonlinear muskingum routing. *Journal of Hydrology* **205**, 52–65.

Birkhead, A. L. & James, C. S. 2002 Muskingum river routing with dynamic bank storage. *Journal of Hydrology* **264**, 113–132.

Bosilovich, M. G., Runhua, Y. & Houser, P. R. 1999 River basin hydrology in a global off-line land-surface model. *Journal of Geophysical Research* **104** (D16), 19661–19673.

Bulletin of Water Resources in China 2000 http://www.mwr.gov.cn/zwzc/hygb/szygb/qgszygb/, in Chinese (accessed 18 April 2013).

Camacho, L. A. & Lees, M. J. 1999 Multilinear discrete lag-cascade model for channel routing. *Journal of Hydrology* **226**, 30–47.

Coe, M. T., Costa, M. H. & Howard, E. A. 2008 Simulating the surface waters of the Amazon River basin: impacts of new river geomorphic and flow parameterizations. *Hydrological Processes* **22**, 2542–2553.

Cunge, J. A. 1999 1. Accuracy criteria for linearised diffusion wave flood routing by K. Bajracharya and D. A. Barry [*Journal of Hydrology*, 195(1997), 200–217]; 2. Similarity of kinematic and diffusive waves: a comment on paper (1) by R. Szymkiewicz. *Journal of Hydrology* **216**, 254–256.

Dai, A. & Trenberth, K. E. 2002 Estimates of freshwater discharge from continents: latitudinal and seasonal variations. *Journal of Hydrometeorology* **3**, 660–687.

Dai, Y., Zeng, X., Dickinson, R. E., Baker, I., Bonan, G. B., Bosilovich, M. G., Denning, A. S., Dirmeyer, P. A., Houser, P. R., Niu, G., Oleson, K. W., Schlosser, C. A. & Yang, Z.-L. 2003 The Common Land Model. *Bulletin of the American Meteorological Society* **84**, 1013–1023.

Döll, P. & Lehner, B. 2002 Validation of a new global 30-min drainage direction map. *Journal of Hydrology* **258**, 214–231.

Döll, P. & Siebert, S. 2002 Global modeling of irrigation water requirements. *Water Resources Research* **38**, 1037–1046.

Davies, H. N. & Bell, V. A. 2009 Assessment of methods for extracting low-resolution river networks from high-resolution digital data. *Hydrological Sciences Journal* **54**, 17–28.

Du, J., Xie, H., Hu, Y., Xu, Y. & Xu, C.-Y. 2003 Development of a high resolution runoff routing model, calibration and application to assess runoff from the LMD GCM. *Journal of Hydrology* **280**, 207–228.

Du, J., Xie, H., Hu, Y., Xu, Y. & Xu, C.-Y. 2009 Development and testing of a new storm runoff routing approach based on time variant spatially distributed travel time method. *Journal of Hydrology* **369**, 44–54.

Du, J., Xie, H., Hu, Y., Xu, Y. & Xu, C.-Y. 2010 Reply to comment on 'Development and testing of a new storm runoff routing approach based on time variant spatially distributed travel time method' by Du *et al*. [*Journal of Hydrology* 369, (2009), 44–54]. *Journal of Hydrology* **381**, 374–376.

Falloon, P., Betts, R., Wiltshire, A., Dankers, R., Mathison, C., McNeall, D., Bates, P. & Trigg, M. 2011 Validation of River Flows in HadGEM1 and HadCM3 with the TRIP River Flow Model. *Journal of Hydrometeorology* **12**, 1157–1180.

Gong, L., Wid-Nilsson, E., Halldin, S. & Xu, C. Y. 2009 Large-scale runoff routing with an aggregated network-response function. *Journal of Hydrology* **368**, 237–250.

Goteti, G., Famiglietti, J. S. & Asante, K. 2008 A catchment-based hydrologic and routing modeling system with explicit river channels. *Journal of Geophysical Research – Part D – Atmospheres* **114** (D14), D14116 (15 pp).

Gusev, Y. M. & Nasonova, O. N. 2000 An experience of modelling heat and water exchange at the land surface on a large river basin scale. *Journal of Hydrology* **233**, 1–18.

Hanasaki, N., Kanae, S. & Oki, T. 2006 A reservoir operation scheme for global river routing models. *Journal of Hydrology* **327**, 22–41.

Jain, M. K. & Singh, V. P. 2005 DEM-based modelling of surface runoff using diffusion wave equation. *Journal of Hydrology* **302**, 107–126.

Keskin, M. E., Ag, I. & Lu, N. 1997 A simplified dynamic model for flood routing in rectangular channels. *Journal of Hydrology* **202**, 302–314.

Krueger, T., Freer, J., Quinton, J. N., Macleod, C. J. A., Bilotta, G. S., Brazier, R. E., Butler, P. & Haygarth, P. M. 2010 Ensemble evaluation of hydrological model hypotheses. *Water Resources Research* **46**, 1–17.

Krueger, T., Quinton, J. N., Freer, J., Macleod, C. J. A., Bilotta, G. S., Brazier, R. E., Butler, P. & Haygarth, P. M. 2009 Uncertainties in data and models to describe event dynamics of agricultural sediment and phosphorus transfer. *Journal of Environmental Quality* **38**, 1137–1148.

Kshirsagar, M. M., Rajagopalan, B. & Lal, U. 1995 Optimal parameter estimation for Muskingum routing with ungauged lateral inflow. *Journal of Hydrology* **169**, 25–35.

Kumar, D. N., Baliarsingh, F. & Raju, K. S. 2011 Extended Muskingum method for flood routing. *Journal of Hydro-environment Research* **5**, 127–135.

Liu, Y., Freer, J., Beven, K. & Matgen, P. 2009 Towards a limits of acceptability approach to the calibration of hydrological models: Extending observation error. *Journal of Hydrology* **367**, 93–103.

Lohmann, D., Mitchell, K. E., Houser, P. R., Wood, E. F., Schaake, J. C., Robock, J., Cosgrove, B. A., Sheffield, J., Qingyun, D., Lifeng, L., Higgins, R. W., Pinker, R. T. & Tarpley, J. D. 2004 Streamflow and water balance intercomparisons of four land surface models in the North American Land Data Assimilation System project. *Journal of Geophysical Research* **109** (D7), 21.

Mcmillan, H., Freer, J., Pappenberger, F., Krueger, T. & Clark, M. 2010 Impacts of uncertain river flow data on rainfall-runoff model calibration and discharge predictions. *Hydrological Processes* **24**, 1270–1284.

Miller, J. R., Russell, G. L. & Caliri, G. 1994 Continental-scale river flow in climate models. *Journal of Climate* **7**, 914–928.

Nilsson, C., Reidy, C. A., Dynesius, M. & Revenga, C. 2005 Fragmentation and Flow Regulation of the World's Large River Systems. *Science* **308**, 405–408.

Nohara, D., Kitoh, A., Hosaka, M. & Oki, T. 2006 Impact of climate change on river discharge projected by multimodel ensemble. *Journal of Hydrometeorology* **7**, 1076–1089.

Oki, T. & Sud, Y. C. 1998 Design of Total Runoff Integrating Pathways (TRIP) – a global river channel network. *Earth Interactions* **2**, 1–37.

Oki, T. & Kanae, S. 2006 Global hydrological cycles and world water resources. *Science* **313**, 1068–1072.

Oki, T., Agata, Y., Kanae, S., Saruhashi, T., Yang, D. & Musiake, K. 2001 Global assessment of current water resources using total runoff integrating pathways. *Hydrological Sciences Journal* **46**, 983–995.

Oleson, K. W., Lawrence, D. M., Bonan, G. B., Flanner, M. G., Kluzek, E., Lawrence, P. J., Levis, S., Swenson, S. C., Thornton, P. E., Aiguo Dai, M. D., Dickinson, R., Feddema, J., Heald, C. L., Hoffman, F., Lamarque, J.-F., Mahowald, N., Niu, G.-Y., Qian, T., Randerson, J., Running, S., Sakaguchi, K., Slater, A., Stöckli, R., Wang, A., Yang, Z.-L., Zeng, X. & Zeng, X. 2010 Technical description of version 4.0 of the Community Land Model (CLM). *NCAR Technical Note*.

Oleson, K. W., Niu, G. Y., Yang, Z. L., Lawrence, D. M., Thornton, P. E., Lawrence, P. J., Stöckli, R., Dickinson, R. E., Bonan, G. B., Levis, S., Dai, A. & Qian, T. 2008 Improvements to the Community Land Model and their impact on the hydrological cycle. *Journal of Geophysical Research* **113**, G01021.

Paiva, R. C. D., Collischonn, W. & Tucci, C. E. M. 2011 Large scale hydrologic and hydrodynamic modeling using limited data and a GIS based approach. *Journal of Hydrology* **406**, 170–181.

Pappenberger, F., Matgen, P., Beven, K. J., Henry, J.-B., Pfister, L. & Fraipont, De P. 2006 Influence of uncertain boundary conditions and model structure on flood inundation predictions. *Advances in Water Resources* **29**, 1430–1449.

Perumal, M. 1994 Multilinear discrete cascade model for channel routing. *Journal of Hydrology* **158**, 135–150.

Perumal, M., Moramarco, T. & Melone, F. 2007 A caution about the multilinear discrete lag-cascade model for flood routing. *Journal of Hydrology* **338**, 308–314.

Ponce, V. M., Lohani, A. K. & Scheyhing, C. 1996 Analytical verification of Muskingum-Cunge routing. *Journal of Hydrology* **174**, 235–241.

Renssen, H. & Knoop, J. M. 2000 A global river routing network for use in hydrological modeling. *Journal of Hydrology* **230**, 230–243.

Shaw, D., Martz, L. W. & Pietroniro, A. 2005 Flow routing in large-scale models using vector addition. *Journal of Hydrology* **307**, 38–47.

Sheffield, J., Goteti, G. & Wood, E. F. 2006 Development of a 50-year high-resolution global dataset of meteorological forcings for land surface modeling. *Journal of Climate* **19**, 3088–3111.

Singh, V. P. 1996 *Kinematic Wave Modelling in Water Resources: Surface Water Hydrology*. Wiley, New York, 1399 pp.

Sobol', I. M., Turchaninov, V. I., Levitan, Yu. L. & Shukhman, B. V. 1992 *Quasi Random Sequence Generators*. Keldysh Institute of Applied Mathematics, Russian Academy of Sciences, Moscow.

Sperna Weiland, F. C., Van Beek, L. P. H., Kwadijk, J. C. J. & Bierkens, M. F. P. 2010 The ability of a GCM-forced hydrological model to reproduce global discharge variability. *Hydrology and Earth System Sciences Discussions* **7**, 687–724.

Tong, C. 2006 Refinement strategies for stratified sampling methods. *Reliability Engineering & System Safety* **91**, 1257–1265.

Tong, C. 2010 Self-validated variance-based methods for sensitivity analysis of model outputs. *Reliability Engineering & System Safety* **95**, 301–309.

Tong, C. 2011 https://computation.llnl.gov/casc/uncertainty_quantification/index.html.

Westerberg, I. K., Guerrero, J. L., Younger, P. M., Beven, K. J., Seibert, J., Halldin, S., Freer, J. E. & Xu, C. Y. 2011 Calibration of hydrological models using flow-duration curves. *Hydrology and Earth System Sciences* **15**, 2205–2227.

Wisser, D., Fekete, B. M., Vörösmarty, C. J. & Schumann, A. H. 2010 Reconstructing 20th century global hydrography: a contribution to the Global Terrestrial Network- Hydrology (GTN-H). *Hydrology and Earth System Sciences* **14**, 1–24.

Yanli, L., Jim, F., Keith, B. & Patrick, M. 2009 Towards a limits of acceptability approach to the calibration of hydrological models: extending observation error. *Hydrology* **367**, 93–103.

Ye, A., Xia, J. & Wang, G. 2005 Drainage network extraction and subcatchment delineation based on digital elevation model. *Journal of Hydraulic Engineering* **36**, 531–537.

Ye, A., Xia, J. & Wang, G. 2006 A distributed kinematic routing model based on dynamical networks. *Yellow River* **2**, 26–28.

Yen, B. C. & Tsai, C. W. S. 2001 On noninertia wave versus diffusion wave in flood routing. *Journal of Hydrology* **244**, 97–104.

Zhang, S., Cordery, I. & Sharma, A. 2002 Application of an improved linear storage routing model for the estimation of large floods. *Journal of Hydrology* **258**, 58–68.

First received 22 October 2011; accepted in revised form 18 May 2012. Available online 7 November 2012